CERN
CH 1211 Geneva 23
Switzerland

Technical Note

EST-ESI/2000-007
ST-2000-059

MECHANICAL ANALYSIS AND OPTIMISATION OF LARGE AND HIGHLY-LOADED BEARING ROLLERS FOR THE "RIESENRAD" ION GANTRY

Maciej Krasinski[*] & Stefan A. Reimoser[**]

Abstract

A carbon ion gantry would allow the irradiation of cancer patients with carbon ions from any direction in space best suited for therapy. Till today, such a machine has not been built due to the expected size, mass and cost. A novel design, called "Riesenrad" ion gantry, promises to provide a competitive solution. The central part of the Riesenrad, which can rotate ± 90°, is supported (statically determinate) on pendular bearing units with two rollers each. High precision requirements for the structure rule out any plastic deformations in the area of contact. The present report describes the design of the highly-loaded rollers. In order to achieve a large contact area and a uniform distribution of contact stresses, a "barrel shape" for the rollers is proposed. An analysis using the finite element method (FEM) was performed to optimise the roller design, namely to establish the required crown roll (camber radius).

Keywords: ion gantry, bearing rollers, contact stress, Hertz stress, roller design, finite element method

August 2000

[*] Cracow University of Technology, Poland
[**] CERN ST and Institute of Industrial Building, Vienna Univ. of Technology, Austria

Distribution: See list
Secretariat: EST-ESI/*Liliane Olivier*

Table of Contents

List of figures

List of tables

1. INTRODUCTION

The paper deals with the design and optimisation of large and highly loaded cylindrical rollers. The initial need for such a type of bearing roller came up during the design of the so-called "Riesenrad" ion gantry, which was investigated in the framework of the CERN-hosted Proton-Ion Medical Machine Study (PIMMS). The study aimed at the design of a generic facility for cancer treatment with protons and carbon ions, focusing in particular on the medical accelerator and later also on the carbon-ion gantry - a structure offering the possibility to deliver a carbon ion beam from any direction in space towards a supine patient with a sub-millimetre accuracy [1].

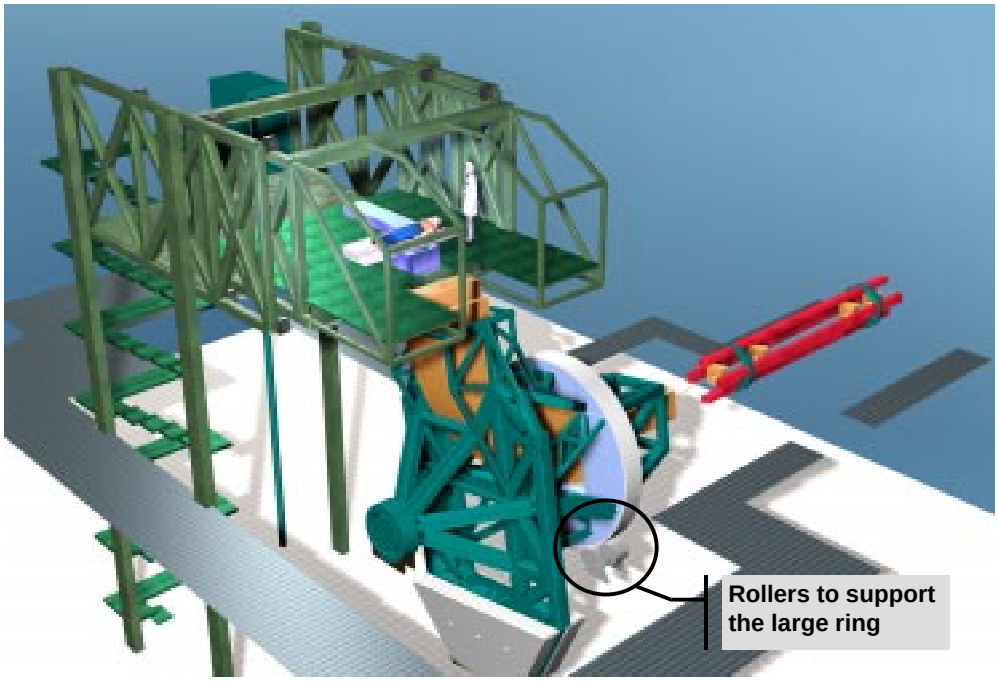

Figure 1 - Perspective view of the proposed Riesenrad ion gantry. The large front ring is supported by two pendular bearing units equipped with two rollers each (statically determinate support).

The proposed design is shown in Figure 1. It is driven by the desire to minimise the elastic deformation of the structure along the beam path. Four rollers support a large ring and each of them has to withstand a radial force of 250 kN (service condition). However, plastic deformation in the contact area between roller and large ring should be strictly avoided since such plastic deformations would possibly:

- modify the geometry of the gantry in an unknown way and by that affect adversely the gantry alignment precision,
- in the long term deteriorate the surface of the large ring.

Consequently, the objectives of this study were:

- First, to check *analytically* for a section perpendicular to the axis of roller rotation that the equivalent stresses in the (perfectly supported) contact zone do not exceed the yield strength of the steel.

- Second, to establish the geometry necessary in the third dimension, namely the radius of the crown roll (camber), in order to achieve a smooth stress distribution (if possible) over the whole length of the roller.

  If the FEM study indicated non-satisfying bearing capacity of the roller the possible mitigation strategies would be:

- Increase the diameter of the rollers, which would lead to strong geometrical inconveniences in the gantry design.
- Surface hardening of the rollers and the large ring. However, for the latter this seems difficult and expensive. Additionally, the ring should have a slightly better surface quality than the rollers in order to restrict any potential damage to the (more easily replaceable) rollers.
- Increase the number of rollers. Again, space for additional rollers is scarce. A self-aligning pendular bearing unit with more than two rollers becomes inconveniently large in height (compare for example the impressive "wiffle trees" for the proton gantries installed at the NPTC in Boston [2]).

2. GEOMETRY AND MATERIAL PROPERTIES

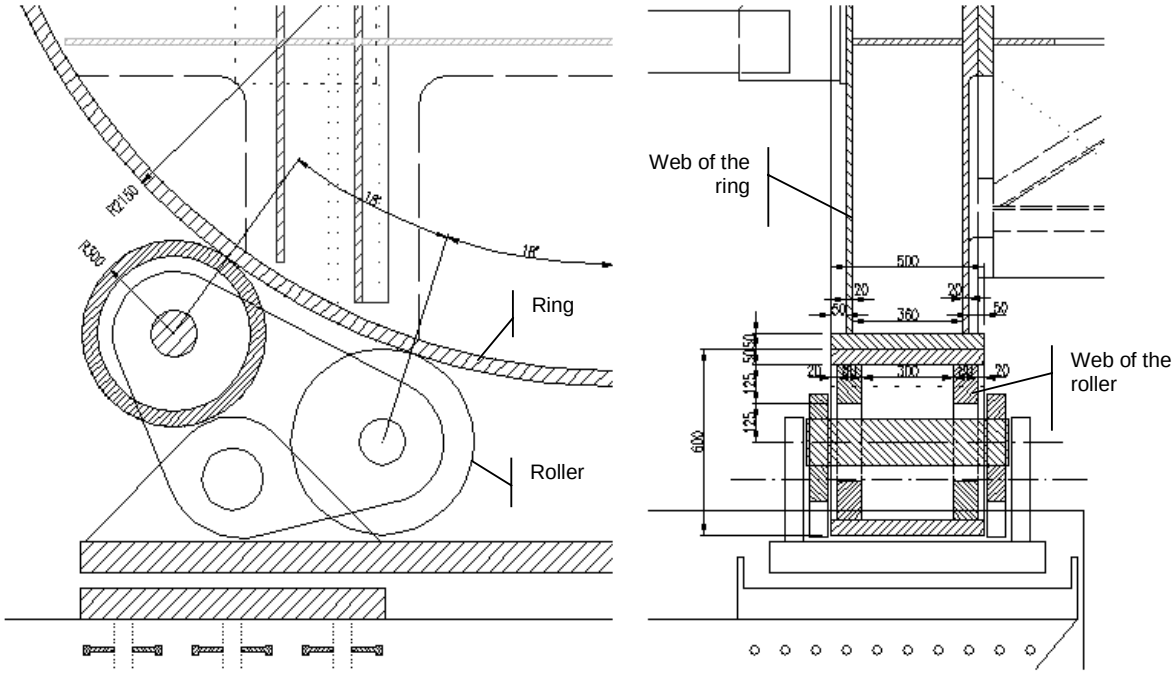

Figure 2 - Geometry of the rollers and the ring. Dimensions are in [mm]

The geometry of the rollers and the ring is shown in Figure 2. Their axes are parallel. The load is supposed to be transferred from the webs of the large front ring onto its rim, then via contact stress onto the rim of the roller and from there via the two webs of the roller towards the supporting roller axis. One web of the ring and one web of each roller always share a common central plane. The material properties are listed in Table 1.

Steel grade	S 355 (Fe 510)
Poisson ratio	0.3
Young's modulus E [N/mm^2]	210000
Yield strength σ_{yield} [N/mm^2]	355 / 335*
Ultimate tensile strength σ_{ult}	510 / 490*
Allowable Hertz pressure [N/mm2]	1000
	* for t > 40 mm

Table 1 - Material properties of the steel foreseen for the rollers and the ring. The values are according to [3]

3. ANALYTICAL CALCULATION OF STRESSES IN THE CONTACT ZONE

As a first approximation of the real situation one can assume ring and rollers to be solid and use Hertz formulas to determine stresses in the contact zone of two long cylinders (having parallel axes). Applying the formulas of [4], as illustrated in Figure 3, the maximum surface pressure in the middle of the contact strip $p_{max} = 264$ N/mm^2. The width of this strip $b = 2.4$ mm. The pressure distribution follows a half circle over b.

Hertz-pressure calculation of the two cylinders (roller and ring) pressed together

Assumption: the cylinders are of large length compared to diameter, axes parallel

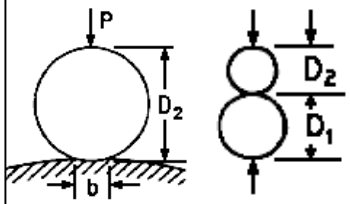

Constants:

$K_D := \frac{D_2 \cdot D_1}{D_2 + D_1}$ $\quad K_D = 526.531 \cdot mm$

$C_E := \frac{1 - \nu_1^2}{E_1} + \frac{1 - \nu_2^2}{E_2}$ $\quad C_E = 8.667 \cdot 10^{-6} \cdot \frac{mm^2}{newton}$

Load per unit length:

$p := \frac{P}{L}$ $\quad p = 500 \cdot \frac{newton}{mm}$

General formulas for width b and σc_{max}:

Width of rectangular contact area:

$b := 1.60 \sqrt{p \cdot K_D \cdot C_E}$ $\quad b = 2.417 \cdot mm$

Compression stress:

$\sigma c_{max} := 0.798 \sqrt{\frac{p}{K_D \cdot C_E}}$ $\quad \sigma c_{max} = 264.15 \cdot \frac{newton}{mm^2}$

Provided that $E_1 = E_2$ and $\nu_1 = \nu_2$, the distance between the centres of the cylinders is reduced by

$2 \cdot p \cdot \frac{1 - \nu_1^2}{\pi \cdot E_1} \cdot \left(\frac{2}{3} + \ln\left(2 \cdot \frac{D_1}{b}\right) + \ln\left(2 \cdot \frac{D_2}{b}\right) \right) = 0.021 \cdot mm$

Figure 3 - Analytical calculation of Hertz stresses and local deformations in the contact zone of roller and ring for the section through the central plane. Ring and roller were assumed to be solid. Formulas according to [4]

Figure 4 shows the distribution of stress components σ_x, σ_y and σ_z and the shear stress $\tau_{45°}$ along the line of symmetry for the two cylinders pressed together assuming a plain strain distribution, which is certainly the case for the central part of the contact area.

For brittle materials, tensile stresses that occur on the surface layer of compressed bodies, close to the area of contact, are responsible for fatigue failure [6]. Ductile materials, however, are likely to fail due to excessive shear stress causing plastification at a depth of $x \approx 0.39\ b$ (in our case about 1 mm below the surface) its value being $\tau_{45} = 0.3\ p_{max}$ (see Figure 4). The comparatively high hydrostatic part of the stress tensor in that point for plain-strain conditions yields comparatively low values for the relevant equivalent (Mises) stress $\sigma_{Mises,\ max} = 0.55\ p_{max}$ [7]. In the present case this value turns out to be $\sigma_{Mises,\ max} = 145$ N/mm^2, i.e. less than half of the yield strength. However, when approaching the edges of the rollers, the plain strain conditions would successively be turned into plain stress conditions and the maximum equivalent stress would rise and eventually become equal to the maximum surface pressure p_{max}.

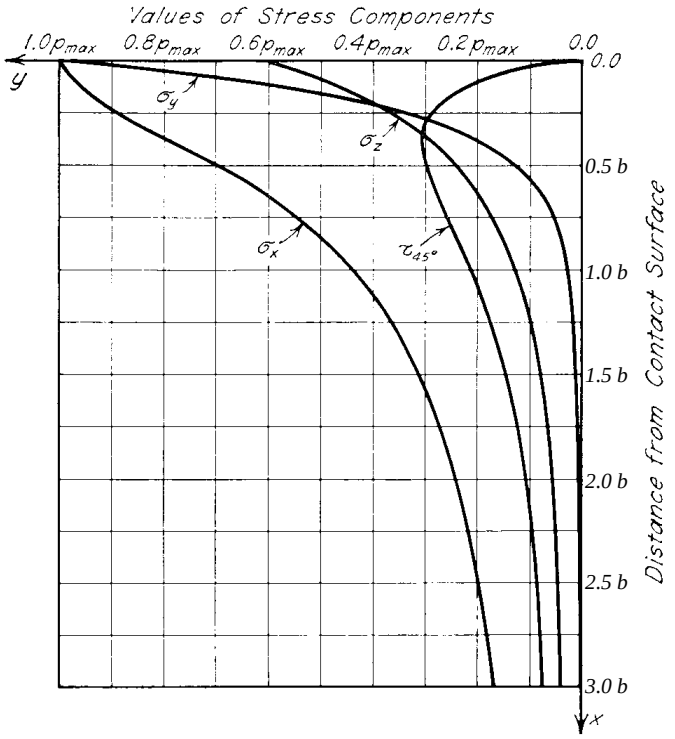

Figure 4 - Distribution of stresses in the contact zone along the line of symmetry for the two cylinders pressed together having parallel axes (similar to [5]), where p_{max} is the maximum contact pressure and b is the (total) width of the contact strip

The results suggest that stresses in the highly loaded contact zone can be kept within the elastic range *provided that the 2D situation analysed above can be achieved uniformly along the entire length of the roller.* However, the assumption that maximum stresses rest unchanged when moving along the (z-) axis of rotation seems doubtful since the rigidity of the roller rim alters considerably when focus is shifted from the comparatively flexible central part towards the more rigid regions close to the webs. In fact the situation resembles - for the ring as well as for the roller - a simply supported girder (with a height equalling the rim thickness) that is resting on the two webs and spanning 380 mm. One would expect that the radial force transferred from the web of the ring towards the one of the roller would cause high contact

stresses in the vicinity of the webs only, hence leaving the rest of the roller surface more or less unloaded.

The theoretical approach to achieve a smooth stress distribution would be to give one of the contact surfaces - reasonably the roller one - a shape that corresponds negatively to its calculated deformed shape. In practice, it is sensible to *give the cylindrical rollers a slightly spherical surface,* i.e. to manufacture them with a crown roll defined by a camber radius, the result is a convex contour or "barrel" roller (see Figure 5). In addition to the smoothed surface-stress distribution one also benefits from an increased ability of the bearing to cope with small misalignments - in particular an expected sagging - of the axis of gantry rotation.

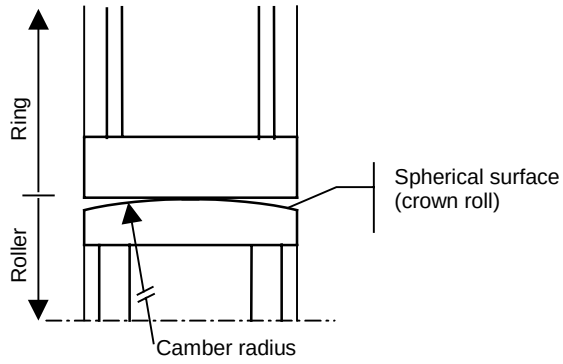

Figure 5 - Ring-roller interface showing schematically the spherical surface of the former cylindrical roller now having a convex contour or "barrel" shape. The "intensity" of this crown roll is defined by a camber radius

As a consequence, analytical Hertz-stress calculations would have to be performed for the more general case of two arbitrarily shaped bodies pressed together (formulas can be found for example in [4]) where each of the two contact surfaces is geometrically modelled by two (mutually perpendicular) principle curvatures. Unfortunately, the formulas do not work when the ratio between the two principal curvatures becomes too large which is the case here.[1] Therefore, it was decided to model and analyse the problem using the finite element method (FEM).

4. 3D MODELLING WITH FINITE ELEMENTS

Due to the high complexity of the task a coarse model was created first with subsequent sub-modelling of the area of interest. The model was built and analysed with the finite element package ANSYS v. 5.5 [8].

4.1 Finite element model

- *3D coarse model using shell elements suited for subsequent sub-modelling.* The model is presented in Figure 6. It consists of the roller and a fragment of the ring modelled by shell elements (type SHELL63). Only half of the real object is modelled due to symmetry. There are contact (interface) elements (CONTAC49) between the rims of the roller and the ring. The number of elements is about

[1] The major semi-axis of the contact ellipse approaches a maximum value of about 90 mm even when the larger radii of curvature of the two bodies approach infinity (modelling two cylinders).

35000. Model edges in the plane of symmetry are restrained in *z*-direction, the free edges of the web of the ring are restrained in radial (top edge) or circumferential direction. A radial force of 125 kN is applied as a distributed load along the inner radius of the roller. The model allows the preliminary estimation of nodal forces and equivalent stresses on the contact surface.

- *3D sub-model to obtain more accurate results*. The sub-model shown in Figure 7 is a fragment of the 3D coarse model but consists of 4-nodes volume elements (SOLID45). Contact elements (CONTAC49) are applied between the surfaces of the rims. The model has around 55000 elements and 61000 nodes. Boundary conditions (including loading) for the sub-model are directly created from the coarse model by the ANSYS program. The 3D sub-model gives full information about stress and strain states in the region of interest.

Friction in the contact elements (CONTAC49) is neglected, which decreases the time of calculation without significant influence on the accuracy of the results.

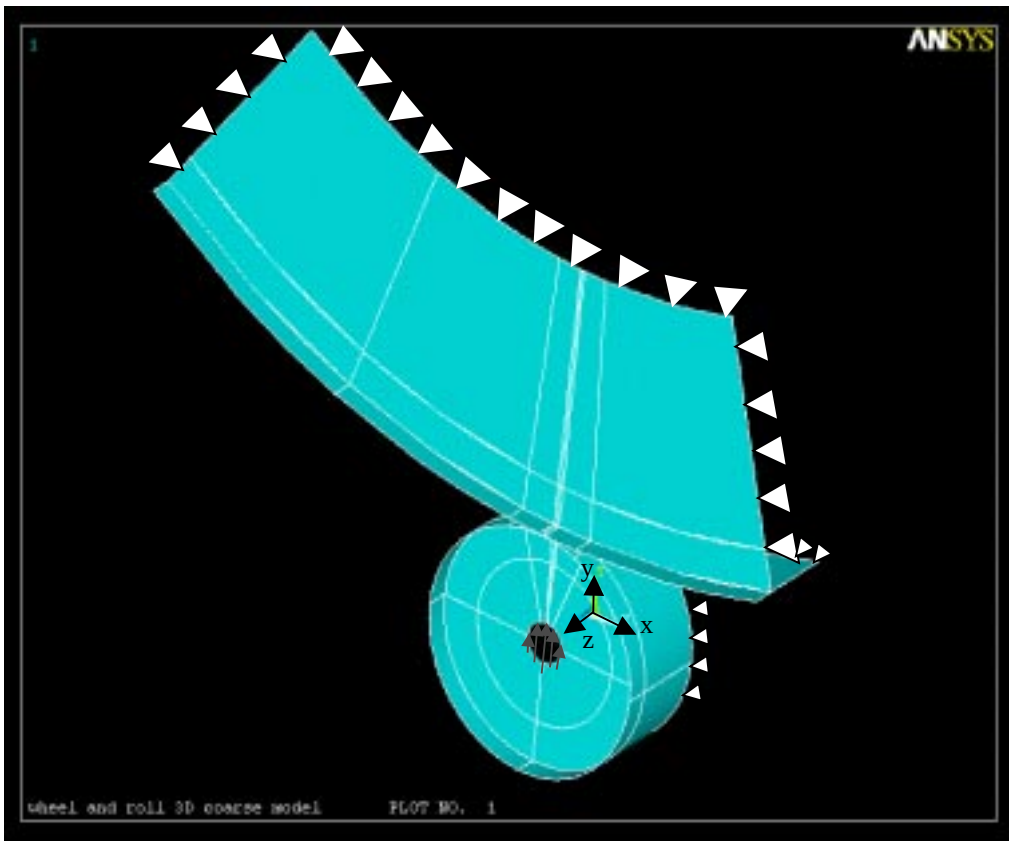

Figure 6 - Coarse model made out of shell elements. Contact elements were put in the interface zone. Boundary conditions (white), loads (red) and the co-ordinate system are indicated.

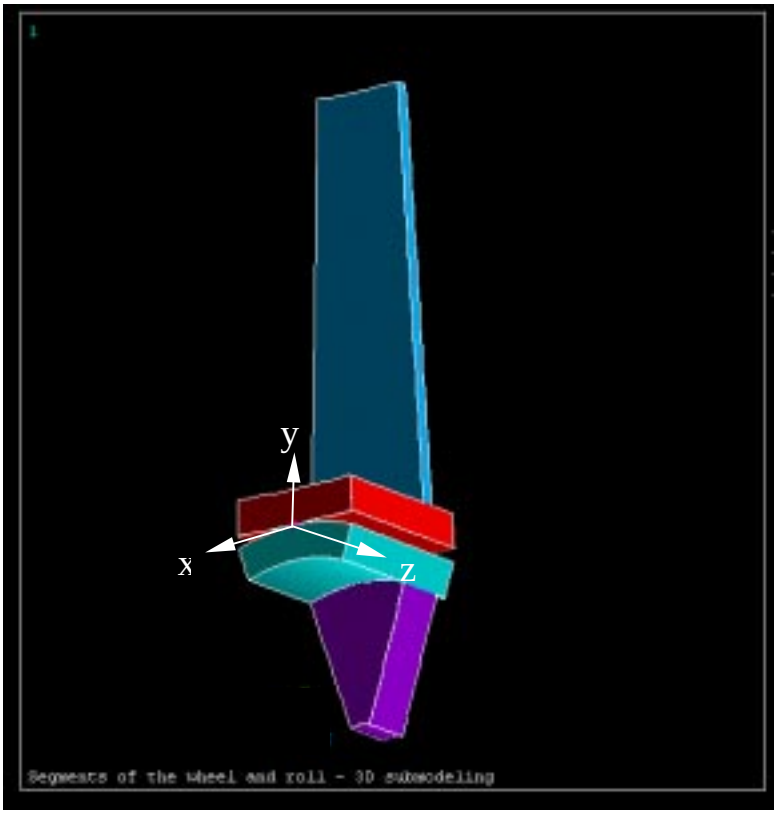

Figure 7 - The sub-model including loads and the co-ordinate system

4.2 Results of computation

Figure 8 gives a *qualitative* idea of how the contact area and the surface pressure vary with different radii of the camber radius (r = 30, 45, 60 m), calculated with the coarse model. Because shell elements were used, the vertical axis indicates *nodal* forces (and not stresses) perpendicular to the contact surface. The horizontal axis (*Z*) indicates the major semi-axis of the contact ellipse. As expected, the maximum normal nodal force decreases with increasing camber radius, showing a corresponding increase in length of the contact area. A small camber radius, i.e. a compact barrel roller, gives a spot-like contact zone in the middle of the roller surface. With increasing radius, the contact pressure becomes more uniformly distributed over a larger area. However, one immediately recognises a growing influence of the webs on the stress distribution in the contact area, leading to considerably higher stress levels at the edges of the contact zone than they are in the centre. Eventually, this contact zone would become separated into two zones where the forces are transferred directly form one web into the other. As can be seen from Figure 8 a camber radius of about 60 m seems to be a good compromise.

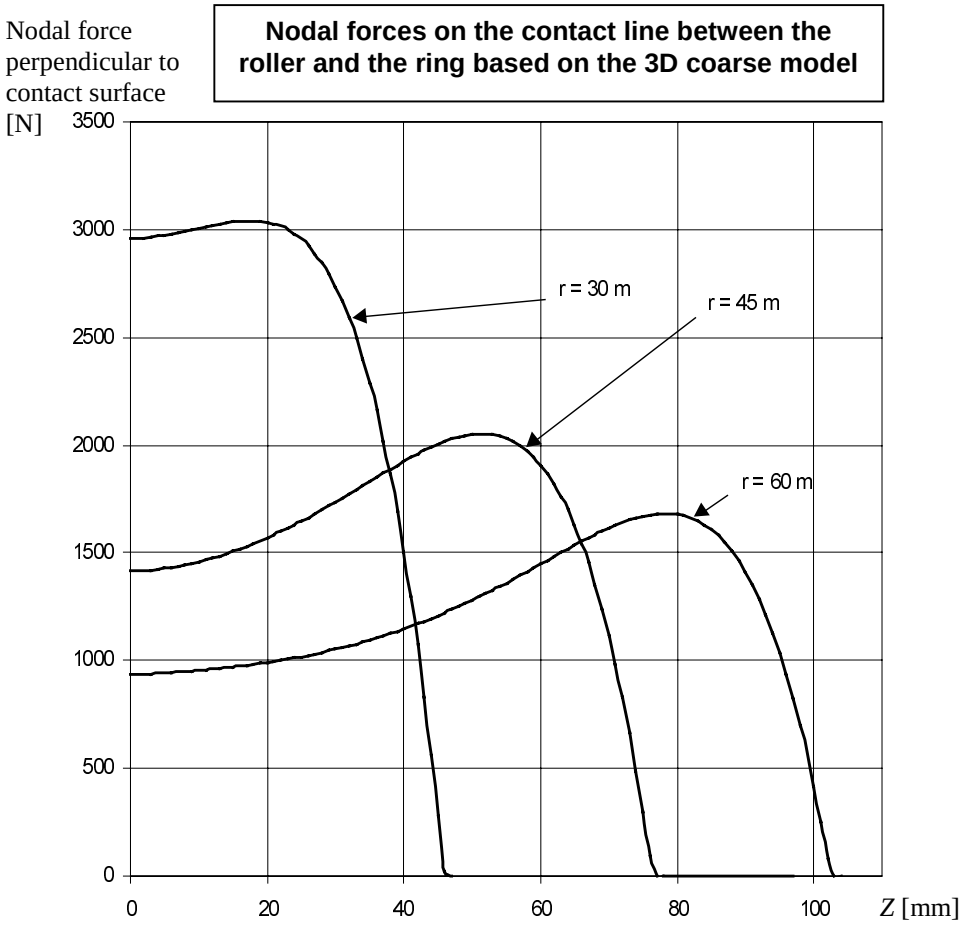

Figure 8 - Nodal forces on the contact line between the roller and the ring calculated from the 3D coarse model. *Z* is parallel to the axis of roller and ring rotation

Table 2 presents the major results of computation for the 3D sub-model for the different camber radii of 30, 45 and 60 m respectively. Note the modified co-ordinate system in the sub-model as indicated in Figure 7 (compared to the analytical calculations): now the *y*-axis is perpendicular to the contact area and *[x-z]* form a plane parallel to the contact area. Due to the size of the elements used in the web modelling, the calculated stresses in the webs are only valid if the filet radius between the web and the rim is larger than about 5 mm.

		Axial curvature radius of the roller in [m]		
		30	45	60
Semi-axes of the contact ellipse [mm]	X-axis	4.0	4.0	3.9
	Z-axis	93	122	150
Maximum contact pressure p_{max} between ring and roller rims in [N/mm^2]		-398	-322	-278
Maximum equivalent (Mises) stress in the rim and the webs of roller and ring in [N/mm^2]	Roller rim	218	163	156
	Roller web	48	50	52
	Ring rim	193	142	132
	Ring web	45	45	45

Table 2 - Principle results of the FEM-analysis of the sub-model

The following issues - all with respect to the 60 m camber radius - merit further attention:

- The major axis of the contact ellipse is about 50% larger than calculated for the coarse model. This is due to the fact that the shell elements used in the coarse model obey the Bernoulli-Euler hypothesis and hence the model is more rigid than the 3D sub-model using brick elements, which are, however, more adequate for evaluating contact problems. The contact area is 300 mm long which is exactly the free span between the two roller webs.
- The minor axis of the contact area turns out to be much longer than predicted by the analytical Hertz pressure calculations, 7.8 mm (!) compared to 2.4 mm respectively, while undergoing similar maximum contact pressures (see Figure 9). Consequently, the general stress situation is far less critical than expected and in fact it is due to this broadened contact area that maximum contact stresses are not exceeding the yield stress of the material although not all the 500 mm of the roller breadth are in contact. One reason for this dramatic increase of the contact breadth is that the FEM analysis takes into account *global* deformations (due to the elasticity of the *structures*) whereas the Hertz calculations are based on the Saint-Venant's principle, i.e. only the *local* deformations are considered.
- The contact area forms an ellipse of 150 mm $\times$ 3.9 mm $\times \pi$ = 1838 mm^2, giving an average contact pressure of 136 N/mm^2.
- The maximum surface pressure $p_{\max}$ (= $\sigma_{y,\,max}$) is 278 N/mm^2 i.e. about twice the average value. The pressure distribution on a radial half-slice of the roller rim (cut through the centre point of the contact area) is illustrated in Figure 10. The same values were observed on the contact surface of the ring rim.
- The equivalent (Mises) stresses for the crucial slice in the rims are presented in Figure 11. They show a similar distribution as for the surface pressure. The maximum equivalent stress occurs already close to the webs and *on* the surface. Obviously, the model does not behave in a classical Hertz-pressure manner anymore (whereas for the 30 m camber radius the maximum Mises stress was observed at the centre and slightly *below* surface.)
- Equivalent (Mises) stresses in the webs are non-critical. The maximum value for the 20 mm web of the ring is about 45 N/mm^2.
- According to analytical Hertz-pressure assumptions, σ_y and σ_x should be equal, but they are 278 N/mm^2 and 188 N/mm^2 respectively. Again the probable reason is that the Hertz-pressure calculations refer to the contact of two infinite elastic bodies, which are more rigid in circumferential direction than the rims of the roller and the wheel. σ_z almost exactly has the value predicted in the analytical section, i.e. $0.6 \times \sigma_y$ = 166 N/mm^2.

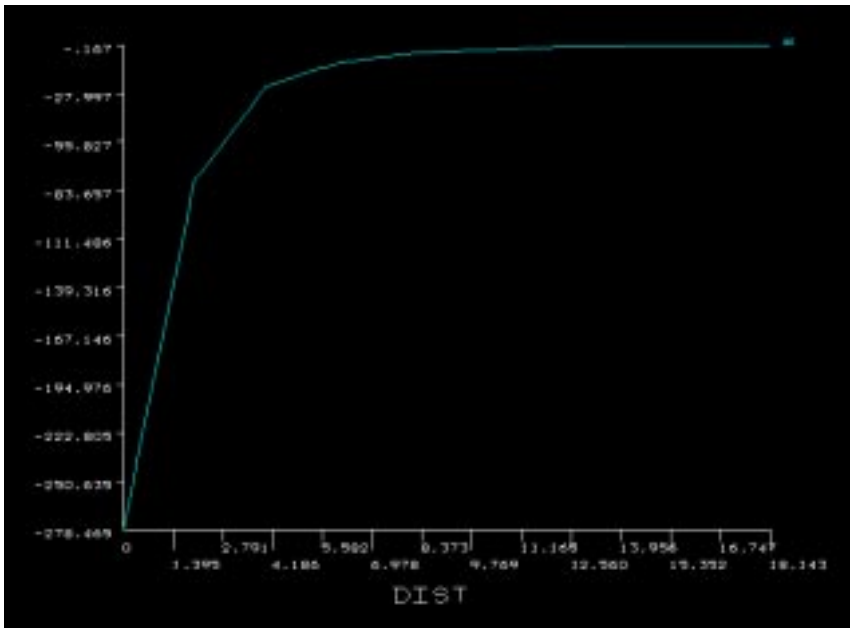

Figure 9 - Contact pressure σ_y [N/mm^2] plotted along the circumferential direction of the roller (*x*-direction in the sub-model [mm]) starting from the centre of the contact area. The total length of the minor semi-axis of the contact ellipse is approximately 4 mm.

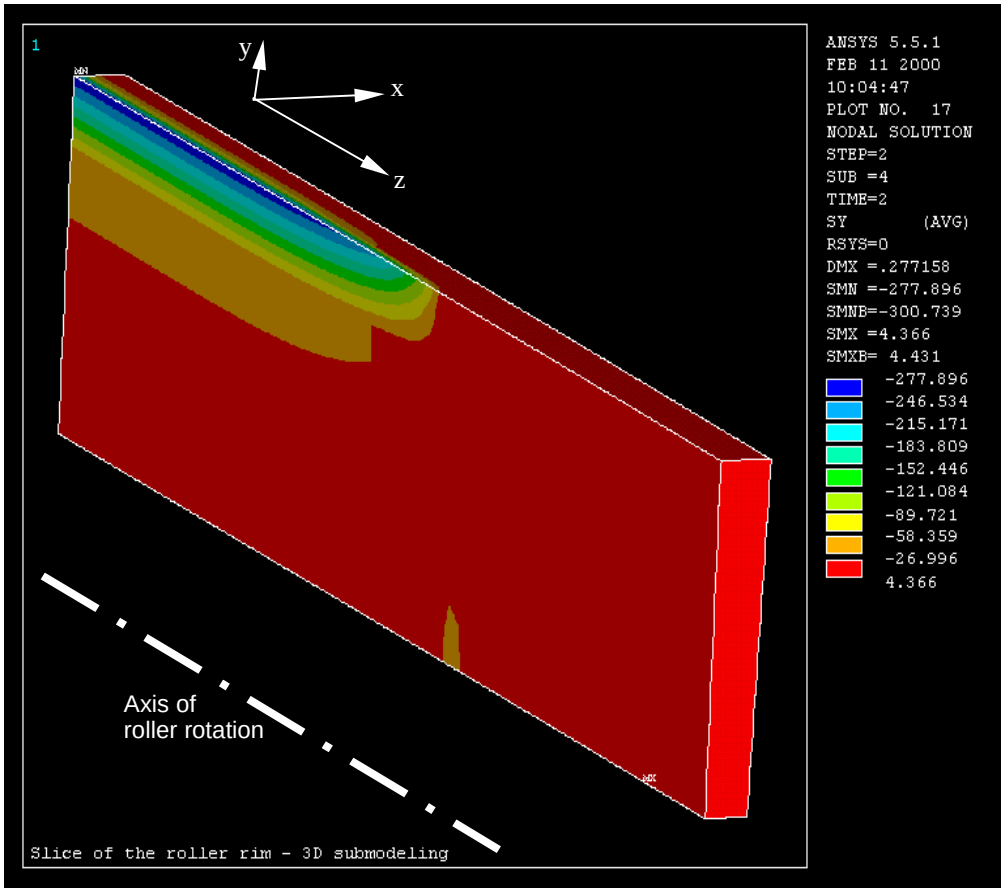

Figure 10 - Distribution of the contact pressure (σ_y in the sub-model) on a radial half-slice of the roller rim which was cut through the centre point of the contact area

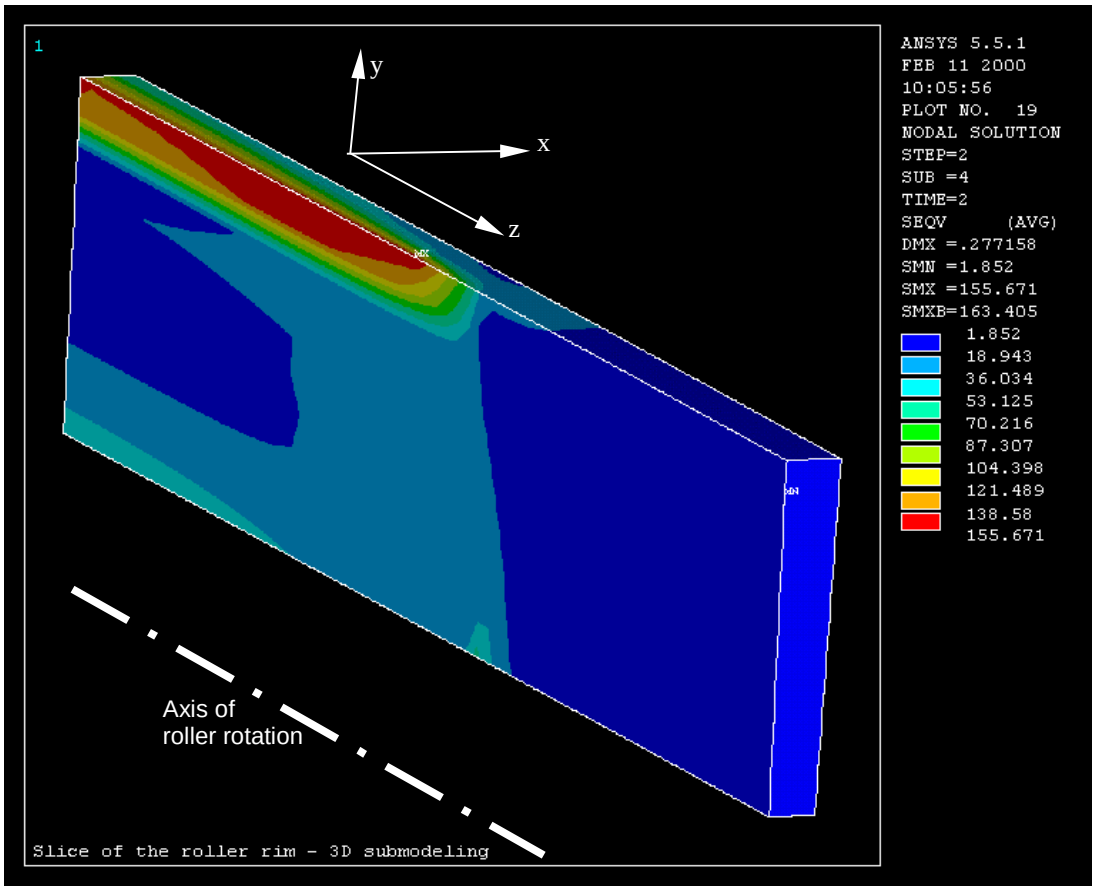

Figure 11 - Distribution of σ_{Mises} (equivalent stress) along a radial half-slice of the roller rim that was cut through the centre point of the contact area. The maximum value occurs close to the web and on the surface. At the bottom, the influence (and hence the position) of the roller web is visible

5. CONCLUSIONS

On the basis of the results obtained by means of the finite element method (FEM), the following conclusions can be made:

- To give the rollers a slightly spherical shape (i.e. to manufacture them applying a camber radius to achieve a barrel type shape) is a useful measure to smooth the stress distribution in the roller-ring interface. It also helps to avoid stress concentration on the roller edges in case of a slight misalignment of the axis of rotation.
- A camber radius of around 60 m - perhaps slightly higher - seems to give a maximised contact area while still keeping contact stresses comparatively uniform.
- Provided that a contact breadth as computed in the FEM analysis can be achieved, maximum equivalent stresses calculated are 155 N/mm^2, i.e. well below the value of the yield point of 355 N/mm^2 hence suggesting a considerable bearing reserve for the contact zone.
- The maximum surface pressure calculated is 280 N/mm^2 (camber radius 60 m). If this value is interpreted as a Hertz pressure, it is acceptable and far away from the allowable maximum quoted in Table 1 (1000 N/mm^2). Obviously, such a high

allowable surface pressure refers to classical Hertz pressure calculations and do already take into account several beneficial effects occurring in real situations like increased contact breadth due to global deformations, surface hardening and plain strain conditions in the contact area.

- The influence of the camber radius on the equivalent stresses in the webs can be neglected.
- In a revised design the following changes in geometry should be discussed: the thickness of the roller webs could be decreased and, as a consequence, one could reduce the length of rollers. In particular, the distance between web and outer edge should be minimised since this outer part of the rim does not contribute to the transfer of forces. If there is a severe lack of space in the bearing unit, the diameter of the roller could be slightly decreased without running into major problems. In contrast, an increase in rim thickness of roller and ring is strongly recommended in order to enhance the smoothing of the surface stress.

6. REFERENCES

[1] Badano L, Benedikt M, Bryant P J (study leader), Crescenti M, Holy P, Maier A, Pullia M, Reimoser S, Rossi S, Borri G, Knaus P, Proton-Ion Medical Machine Study (PIMMS), CERN yellow report, CERN-2000-006, in press, CD-rom available, Part II, Chapter 6

[2] Reimoser S, "Protonengantries" in: Pötter R, Auberger T, Regler M, (eds.): Med-AUSTRON Feasibility Study, Med-AUSTRON Planning Office, c/o RIZ, Stephan-Koren-Strasse 10, A-2700 Wiener Neustadt, December 1998, Section II.3.1.

[3] Schneider K J (ed.), Bautabellen für Ingenieure, Werner Verlag, 12th edition, 1996, p. 8.113

[4] Roark's Formulas for Stress & Strain, Vol. I, McGraw-Hill, 6th edition, 1989, in the version of: Electronic Book in MathCAD, Warren C Young, MathSoft Inc.

[5] Radzimovsky E I, Stress Distribution and Strength Conditions of Two Rolling Cylinders Pressed Together, Eng. Experiment Station, Univ. of Illinois, Bull. 408, 1953, p. 13

[6] Czichos H (ed.), Hütte: Die Grundlagen der Ingenieurwissenschaften, 29th edition, 1989, p. E100

[7] Radzimovsky E I, op. cit., p. 16

[8] ANSYS Analysis Guides version 5.5, 001083, 2nd Edition, SAS IP Inc.